The First Magnetic Fields

George Davies and Lawrence M. Widrow[1]

Department of Physics, Queen's University, Kingston, Ontario, Canada K7L 3N6

ABSTRACT

We demonstrate that the Biermann battery mechanism for the creation of large scale magnetic fields can arise in a simple model protogalaxy. Analytic calculations and numerical simulations follow explicitly the generation of vorticity (and hence magnetic field) at the outward-moving shock that develops as the protogalactic perturbation collapses. Shear angular momentum then distorts this field into a dipole-like configuration. The magnitude of the field created in the fully formed disk galaxy is estimated to be 10^{-17} Gauss, approximately what is needed as a seed for the galactic dynamo.

Subject headings: galaxies: magnetic fields — formation — hydrodynamics — methods: nbody simulations

1. Introduction

The origin of galactic magnetic fields has proved to be one of the most challenging and stubborn problems in modern astrophysics (Rees 1987; Kronberg 1994 and references therein). It is generally assumed that galactic fields are generated and maintained by the dynamo action of a differentially rotating disk galaxy. However, a dynamo can only amplify an existing field and so the question of galactic magnetic fields splits naturally into two parts: creation of the field required to seed the dynamo, and the nature of the dynamo itself (e.g., Zel'dovich, Ruzmaiken, & Sokoloff 1983).

An early attempt to explain the origin of seed fields is due to Harrison (1970, 1973) who showed that magnetic fields are created during the radiation era if significant vorticity exists at that epoch. However, primordial vorticity in an expanding universe decays with time (in contrast with the irrotational density perturbations presumably responsible for structure formation). Indeed, the absence of significant vorticity prior to galaxy formation together with the observation that vorticity is generic to galactic disks may provide an important clue as to the origin of galactic magnetic fields. Angular momentum in galaxies is thought to arise from tidal torques among neighboring protogalaxies (Hoyle 1949, Peebles 1969, and White 1984). However, gravitational forces alone do not produce vorticity and therefore its appearance must be due to 'gasdynamical' processes such as those that occur at oblique shocks. These same processes also produce magnetic

[1]Visiting Professor, Department of Astronomy and Astrophysics, University of Chicago

fields by creating a so-called Biermann battery (Biermann 1950) which drives electric currents in the plasma. Since oblique shocks are inevitable in collapsing gas clouds, the early stages of structure formation provide a natural site for the production of seed fields (Pudritz & Silk 1989, Kulsrud et al. 1997).

There have, of course, been other attempts to explain the origin of seed fields. One possibility is that first fields were created in stars and subsequently expelled into the interstellar medium (Bisnovatyi-Kogan, Ruzmaiken, & Syunyaev 1973). Alternatively, seed fields may have been created in the very early Universe through such exotic phenomena as quantum field creation during inflation (Turner and Widrow 1988, Ratra 1992), phase transitions (Quashnock, Loeb, & Spergel 1988, Vachaspati 1991, Field & Carroll 1998), and topological defects (Sicotte 1997). By comparison, the protogalactic battery has a certain simplicity and elegance since the necessary ingredients are generic to models of galaxy formation.

Most discussions of galaxy formation ignore the influence of magnetic fields (see, however Wasserman 1978 and Kim, Olinto, & Rosner 1996). To be sure, galactic magnetic fields play an important role in a number of astrophysical processes such as star formation, cosmic ray confinement and gasdynamics. But while the energy density in galactic magnetic fields is comparable to that in cosmic rays and in the turbulent motion of the interstellar medium, it is considerably less than the energy density associated with the global dynamics of a galaxy. This suggests that magnetic fields play a secondary role in the formation and evolution of galaxies. Nevertheless, models of galaxy formation should be able to explain their origin.

In this work, we investigate the generation and early evolution of vorticity and magnetic fields in the context of a detailed, albeit highly idealized, model protogalaxy. Recently, Kulsrud et al. (1997) have attempted to follow the creation of protogalactic magnetic fields in a cosmological hydrodynamic simulation of a cold dark matter universe. They find that seed fields can be produced on a variety of cosmologically interesting scales. Our work complements and enhances theirs by considering a simpler system where both analytic and numerical techniques can be employed. In so doing, we are able to understand these earlier results and some of their limitations in terms of relatively simple physics and numerics. Our work also makes contact with various semi-analytic models of disk galaxy formation.

An outline of our scenario is as follows:

- We consider an isolated, nearly spherical, density perturbation in an otherwise Einstein-de Sitter universe. The cosmic fluid consists of both collisional gas and collisionless dark matter. We assume that the scales of interest are significantly smaller than the horizon so that a Newtonian treatment is adequate.

- Each element in the fluid expands to a maximum or turnaround radius (as measured from the center of the protogalaxy) before collapsing with inner regions reaching turnaround first. It is during the early stages of collapse that an outward moving shock develops. As infalling

material passes through the shock, it is heated rapidly and decelerated.

- Vorticity is generated at the shock provided the velocity of the infalling gas is not everywhere perpendicular to the shock surface. We demonstrate this for an axisymmetric prolate protogalaxy where the vorticity generated at the shock is in the azimuthal direction.

- An external tidal torque applied to the protogalaxy generates shear angular momentum which in turn couples to the vorticity in the postshock region. As an example we consider again the model protogalaxy described above but now under the influence of a tidal torque along one of its short axes. The resultant shear field couples to the vorticity generated at the shock to yield a large-scale dipole-like vorticity field oriented along the direction of the tidal torque, i.e., along what will ultimately be the spin axis of the galaxy. The concomitant magnetic field has the same geometry and provides the seed field for subsequent dynamo action.

Most previous analyses of protogalactic field generation have sought order of magnitude estimates for the seed field strength without making direct contact to specific models of structure formation (Pudritz & Silk 1989; Lesch & Chiba 1994). Our results are in agreement with these estimates and go one step further by providing a clear and simple picture of the geometry of the seed field. Our model is in the spirit of the semi-analytic and numerical studies of disk galaxy formation by Mestel 1963; Fall & Efstathiou 1980; Katz & Gunn 1991; Dalcanton, Spergel, & Summers 1997 and others. However, in those works, angular momentum and vorticity are assumed *ab initio* and they are therefore unable to shed light on the creation of the first magnetic fields. In contrast, our model explicitly follows vorticity generation during the earliest stages of galaxy formation.

In Section 2 we review the vorticity-magnetic field connection, derive an expression for the magnetic field generated at an oblique shock, and apply the results to our model protogalaxy. These analytic calculations are enough to obtain an estimate for the magnitude of the magnetic field as well as the general features of its geometry. The numerical simulations presented in Section 3 provide a check of these results and also serve to illustrate some of the pitfalls inherent in using simulations to study problems of this type. These simulations do not include angular momentum and so in Section 4, we present a simple semi-analytic calculation for the postshock evolution of the vorticity and magnetic field in the presence of shear angular momentum. We conclude, in Section 5, with a summary and discuss directions for future work.

2. Vorticity Generation in a Protogalaxy: Analytic Treatment

2.1. Vorticity-Magnetic Field Connection

The evolution of a collisional fluid is described by the Euler equation

$$\frac{\partial \mathbf{v}}{\partial t} + (\mathbf{v} \cdot \boldsymbol{\nabla})\, \mathbf{v} \;=\; -\frac{1}{\rho}\boldsymbol{\nabla} p - \boldsymbol{\nabla}\psi \tag{1}$$

together with Poisson's equation for the gravitational potential ψ, the continuity equation, an equation of state, and an energy equation. Taking the curl of eq. 1 yields the following for the vorticity $\boldsymbol{\omega} \equiv \boldsymbol{\nabla} \times \mathbf{v}$:

$$\frac{\partial \boldsymbol{\omega}}{\partial t} - \boldsymbol{\nabla} \times (\mathbf{v} \times \boldsymbol{\omega}) \;=\; \frac{\boldsymbol{\nabla}\rho \times \boldsymbol{\nabla} p}{\rho^2} \tag{2}$$

Thus, while galaxies can acquire angular momentum through tidal fields, vorticity arises through purely gasdynamical processes, namely pressure and density gradients that are not colinear.

Biermann (1950) realized that a similar situation exists for magnetic fields. In the usual formulation of magnetohydrodynamics (MHD), the evolution of a magnetic field is described by the equation

$$\frac{\partial \mathbf{B}}{\partial t} - \boldsymbol{\nabla} \times (\mathbf{v} \times \mathbf{B}) - \frac{c^2}{4\pi\sigma}\nabla^2 \mathbf{B} = 0 \tag{3}$$

where σ is the conductivity. If $\mathbf{B}$ is initially zero, then it will be zero at all times. However, the derivation of eq. 3 assumes a form for Ohm's law that is not strictly valid for an electron-ion fluid. A careful treatment dictates that we include, on the right hand side, the term

$$\boldsymbol{\Gamma} = \frac{c}{e}\frac{\boldsymbol{\nabla} n_e \times \boldsymbol{\nabla} p_e}{n_e^2} \tag{4}$$

where n_e and p_e are the number density and pressure of free electrons. Approximate local charge neutrality implies that $n_e \simeq n_p \equiv \chi\rho/m_p$ where n_p is the proton number density, χ is the ionization fraction, and m_p is the proton mass. In addition, since the electron temperature is expected to be approximately equal to the total gas temperature, $p_e \simeq p n_e/\left(n_e + n_p\right) = p\chi/\left(1+\chi\right)$. We can therefore write

$$\boldsymbol{\Gamma} = \alpha \frac{\boldsymbol{\nabla}\rho \times \boldsymbol{\nabla} p}{\rho^2} \tag{5}$$

where $\alpha \equiv m_p c/e\,(1+\chi)\,1.05\times \simeq 10^{-4}\mathrm{Gauss}\cdot\mathrm{s}$ (Kulsrud et al. 1997).

In the limit of vanishing diffusion, the equations for $\boldsymbol{\omega}$ and $\mathbf{B}$ take identical forms. Together with the assumption that initially both the vorticity and magnetic field are zero, we have the relation,

$$\mathbf{B} = \alpha\boldsymbol{\omega} \simeq 10^{-4}\boldsymbol{\omega} \tag{6}$$

where the units of $\mathbf{B}$ and $\boldsymbol{\omega}$ are Gauss and Hz respectively. The growth and evolution of the magnetic field therefore mirrors that of the vorticity up until the time when the diffusive effects of viscosity and conductivity become important[2].

2.2. Shock Wave Preliminaries

For a barytropic fluid, $p = p(\rho)$ and therefore $\boldsymbol{\Gamma} = 0$. However, at curved shocks, the equation of state is more complicated ($p = p(\rho, s)$ where s is the entropy) reflecting the fact that bulk kinetic

[2]See again, Kulsrud et al. (1997) for a further discussion of this point.

energy can be converted to thermal energy. We therefore expect $\mathbf{\Gamma} \neq 0$ and hence the generation of both vorticity and magnetic fields (Kulsrud et al. 1997).

An ideal shock can be treated as a surface of discontinuity in the gas flow. By imposing certain jump conditions at this surface we can derive a relationship between the velocity field of the gas in the pre- and post-shock regions and hence an expression for the vorticity generated at the shock. In this way, we bypass eq. 5 and avoid dealing with the complicated gasdynamics that occurs inside the shock

The standard shock wave jump conditions (e.g., Landau and Lifshitz 1997) consist of a set of three relations that guarantee the conservation of mass, momentum, and energy across the shock. Consider a point on a shock surface with velocity $\mathbf{v}_s$ and normal $\hat{\mathbf{n}}$. Let ρ_0, $\mathbf{v}_0$, p_0, and h_0 be the density, velocity, pressure, and enthalpy in the preshock region and ρ, $\mathbf{v}$, p, and h be the corresponding quantities in the postshock region. The jump conditions are

$$\rho u = \rho_0 u_0 \tag{7}$$

$$p + \rho u^2 = p_0 + \rho_0 u_0^2 \tag{8}$$

$$h + \frac{1}{2}u^2 = h_0 + \frac{1}{2}u_0^2 \tag{9}$$

where u_0 and u are the velocity components along $\hat{\mathbf{n}}$ in the rest frame of the shock:

$$u_0 \equiv (\mathbf{v}_0 - \mathbf{v}_s) \cdot \hat{\mathbf{n}} \qquad u \equiv (\mathbf{v} - \mathbf{v}_s) \cdot \hat{\mathbf{n}} \ . \tag{10}$$

In addition, we have that the component of the velocity tangent to the shock is continuous.

For the situation at hand, the preshock gas is relatively cold and we can therefore set $p_0 \simeq 0 \simeq h_0$. The three jump conditions are then easily combined to give

$$u = \left(\frac{\gamma - 1}{\gamma + 1}\right) u_0 \tag{11}$$

where γ is the polytropic index of the infalling gas (equal to 5/3 for an ideal gas). This allows us to express the velocity in the postshock region in terms of the preshock velocity:

$$\mathbf{v} = \mathbf{v}_0 + (f(\gamma) - 1)u_0\hat{\mathbf{n}} \tag{12}$$

where $f(\gamma) \equiv (\gamma - 1)/(\gamma + 1)$.

2.3. Vorticity in the Postshock Region

The velocity field in the postshock region is determined not only from the initial velocity field and the geometry of the shock (through eq. 12) but also from the evolution of the gas once it has passed through the shock. All of this is incorporated into numerical simulations discussed in the next section. Here we present an analytic model for an idealized protogalaxy. The key simplification

is to ignore the evolution of the gas in the postshock region. Our picture is that the shock wave sweeps through the gas transforming the velocity field from $\mathbf{v}_0$ to $\mathbf{v}$ according to eq. 12 where u_0 and $\hat{\mathbf{n}}$ are evaluated at each point at the instant when the shock passes through. In this way, u_0 and $\hat{\mathbf{n}}$ can be treated as functions of position and we can then calculate the vorticity by taking the curl of $\mathbf{v}$. As discussed above, we expect $\mathbf{v}_0$ to be curl-free so that

$$\boldsymbol{\omega} = (f(\gamma) - 1)\, \boldsymbol{\nabla} \times (u_0 \hat{\mathbf{n}}) \tag{13}$$

To proceed further we require a specific model protogalaxy. As a starting point, we consider the spherical infall model (e.g., Gunn 1975, Gott 1977, Fillmore & Goldreich 1984, Bertschinger 1985, Ryden & Gunn 1987, Ryden 1988) wherein matter is divided into spherical shells which expand to a maximum or turnaround radius and then collapse toward the center. In the case of collisional matter (e.g., Bertschinger 1985) infalling shells are decelerated and heated as they pass through an outward moving shock.

Current theories of structure formation present a far more complicated picture than that represented by the spherical infall model. In particular, structure formation is believed to proceed hierarchically, with subgalactic objects forming first, and then coalescing to form galaxies and clusters. For our purposes, the key deficiency of the spherical infall model is its restriction to spherical symmetry, since this precludes vorticity generation. Moreover, a spherically symmetric protogalaxy cannot acquire angular momentum through tidal torques. Of course, there is no reason to expect protogalaxies to be spherically symmetric. Indeed, the halos found in collisionless N-body simulations are generally triaxial, with prolate shapes favored slightly over oblate ones. Furthermore, the angular momentum vector for these systems is generally aligned with the short axis of the halo (Carlberg & Dubinski 1991; Warren et al. 1992). These results motivate us to consider a simple model protogalaxy that forms from an axisymmetric, prolate density perturbation. An external tidal torque, applied perpendicular to the symmetry axis of the perturbation, generates shear angular momentum. In the spirit of the spherical infall model, we assume that the perturbation is smooth and featureless with a density profile that decreases with radius. The protogalaxy therefore forms from the inside out.

For the moment, we ignore tidal torques. The perturbation will therefore evolve into an axisymmetric protogalaxy. Consider a spherical coordinate system, (r, θ, ϕ), with polar axis oriented along the symmetry axis of the protogalaxy. The density and pressure gradients that occur, for example, at an outward moving shock, will be in the $\hat{\mathbf{r}}$ and $\hat{\boldsymbol{\theta}}$ directions which imply that any vorticity generated will be along the $\hat{\boldsymbol{\phi}}$ direction. Moreover, by symmetry the vorticity above and below the equatorial plane will be in opposite directions. This is not surprising since, in the absence of tidal fields, the net circulation of the system must be zero.

It is instructive to consider a simple ansatz for the evolving protogalaxy. Specifically, we assume that isodensity contours for the gas are concentric spheroids, i.e., $\rho = \rho(\tilde{r}_s)$ where $\tilde{r}_s^2 = r^2 \left(\sin^2\theta + \cos^2\theta/q^2\right)$. q is the flattening parameter which, in general depends on time and radius. For simplicity, we will ignore this complication (we focus on a small region in the neighborhood of

the shock) and further assume that the deviation from spherical symmetry is small ($|q-1| \ll 1$). The shock surface is described by the equation

$$\tilde{r}_s^2(t) \;=\; r^2\left(\sin^2\theta + \cos^2\theta/q^2\right) \tag{14}$$

and the normal to this surface is, to first order in $(q-1)$, given by

$$\hat{\mathbf{n}} = \hat{\mathbf{r}} + 2\,(q-1)\sin\theta\cos\theta\hat{\boldsymbol{\theta}} \tag{15}$$

Thus, one contribution to $\boldsymbol{\omega}$ will be of the form $2\,(f(\gamma)-1)\,(1-q)\,(u_0/\tilde{r}_s)\sin\theta\cos\theta\hat{\boldsymbol{\phi}}$. There is a second contribution that is proportional to $\boldsymbol{\nabla} u_0 \times \hat{\mathbf{n}}$ which has a similar form[3] and we can therefore write

$$\boldsymbol{\omega} \propto (q-1)\,(u_0/\tilde{r}_s)\sin\theta\cos\theta\hat{\boldsymbol{\phi}} \tag{16}$$

The magnitude of the vorticity is therefore set by the velocity of the infalling gas (in the rest frame of the shock) divided by the shock radius. This is roughly equal to the reciprocal of the turnaround time, $T_{\rm ta}$, a result we might have anticipated from dimensional analysis. As a specific example, consider Bertschinger's (1985) solution for secondary infall of collisional matter onto an already collapsed overdensity. In this self-similar model, the turnaround radius at time t is $r_{\rm ta}(t) \propto t^{8/9}$ and the radius of the shock is $r_s(t) = \lambda_s r_{\rm ta}(t)$ where λ_s is a constant $\simeq 0.33$ for $\gamma = 5/3$. Likewise the velocity of the gas, immediately before passing through the shock, is given by $v_0 = -V r_{\rm ta}/t$ where $V \simeq 1.47$ for $\gamma = 5/3$. This implies that $u_0/r_s \simeq 1.7/T_{\rm ta}$.

For a galaxy-sized object, $T_{\rm ta} \sim 10^{16}\,{\rm s}$ and therefore $\omega_\phi \sim 10^{-16}\,{\rm s}^{-1}$. This is roughly a factor of 10 less than the local value of the vorticity in the Milky Way as determined from the Oort constants (e.g., Binney & Merrifield 1998), a reasonable result given that the vorticity will be amplified during the formation of the disk itself. The strength of the corresponding magnetic field is $\sim 10^{-20}$ Gauss. We will return to this result in the next section.

3. Numerical Simulations

In this section we present the results of numerical simulations that are designed to test and augment the analytic model described above. The simulations follow the evolution of an isolated axisymmetric density perturbation in an otherwise flat (Einstein-de Sitter) universe. The cosmic fluid consists of dark matter and gas in a 10:1 ratio. The simulations are performed using HYDRA (Couchman, Thomas, & Pearce 1995): Gravitational forces are calculated with an adaptive particle-particle particle-mesh ($\rm AP^3M$) algorithm while gasdynamics is treated using smooth particle hydrodynamics (SPH). Simulations are run with 32^3 particles of each species.

[3]To evaluate this term, we require an ansatz for the preshock gas flow, $\mathbf{v}_0$. Since this is assumed to be irrotational, it can be written as the gradient of a scalar function. A reasonable ansatz (akin to the Zel'dovich approximation) is $\mathbf{v}_0 \propto \boldsymbol{\nabla}\psi$. In any case, we expect that $\mathbf{v}_0\cdot\hat{\boldsymbol{\theta}}/\mathbf{v}_0\cdot\hat{\mathbf{r}} = O(|q-1|)$ and likewise for $\mathbf{v}_{\rm s}$ so that $u_0 = v_{0r} - v_{sr} + O((q-1)^2)$. Moreover, u_0 should have the form $u_0(r,\theta) = u_0^1 + u_0^2(q-1)\cos^2(\theta)$ where u_0^1 and u_0^2 are functions of r which depend on the details of the model.

The initial density profile has the form $\rho(r,\theta) = \rho_b(t)\,(1+\delta(\tilde{r}))$ where $\rho_b(t)$ is the background density for an Einstein-de Sitter Universe, $\tilde{r} = r\left(\sin^2\theta + \cos^2\theta/q^2\right)^{1/2}$, and

$$\delta(r) = \begin{cases} \delta_0\left(1 - \frac{\alpha}{\alpha+2}\left(\frac{r}{r_c}\right)^2\right) & r < r_c \\ \delta_0\left(\frac{2}{\alpha+2}\left(\frac{r}{r_c}\right)^\alpha\right) & r_c < r < R \end{cases} \tag{17}$$

To set up initial conditions, we begin with an interlaced lattice of gas and dark matter particles. Those particles a distance R from a chosen center are discarded and the ones that remain are displaced from their original lattice sites so as to achieve the desired density profile. Velocities are then assigned according to the Zel'dovich approximation. In the simulations presented here, $\delta_0 = 1$, $r_c/R = 0.4$, $\alpha = 2$, and for the prolate runs, $q = 1.5$. With this choice of parameters, the mean density enhancement is $\bar{\delta} = 0.377$.

The simulation units are such that the total mass $M = 1$ and Newton's constant $G = 0.0194$. Neither cooling nor star formation are included in the simulations and so there is some freedom in choosing units for dimensional quantities. In conventional models of structure formation, such as the Cold Dark Matter scenario (CDM) and its variants, $\bar{\delta}$ can be identified with the rms mass fluctuation on a scale R:

$$\sigma_M(t) \equiv \langle(\Delta M/M)^2\rangle^{1/2} = (1+z)^{-1}\left(\int \frac{k^2 dk}{2\pi^2} P(k) W^2(kR)\right)^{1/2} \tag{18}$$

where $M \simeq 1.2\times10^{12} h^2 M_\odot\,(R/\mathrm{Mpc})^3$ is the total mass in a sphere of radius R, $P(k)$ is the linear power spectrum for the model, h is the present value of the Hubble parameter in units of $100\,\mathrm{km\,s^{-1}\,Mpc^{-1}}$, z is the redshift and $W(x) = 3\,(\sin x - x\cos x)\,/x^3$ is the top hat window function. Thus, by setting $\sigma_M = 0.377$, we can determine the initial redshift for the simulation, z_i, as a function of M. It is then straightforward to relate simulation units to physical units. This is done, for three representative masses, in Table 1 where, in computing σ_M, we have assumed a spatially flat CDM universe with $h = 0.7$, $\Omega_B = 0.05$, and COBE normalization ($\sigma_8 \simeq 1.7$). The transfer function was calculated using the fitting formula of Eisenstein and Hu (1999).

Figure 1 presents the phase space particle distribution (radius r vs. radial velocity v_r) for the spherical run. We see that the turnaround radius, $r_{\rm ta}$, increases with time. For $r > r_{\rm ta}$, the gas and dark matter particles evolve as a single fluid. For $r < r_{\rm ta}$, the dark matter particles exhibit multiple phase space streams that are characteristic of collisionless infall (cf Figure 10 of Fillmore & Goldreich 1984 and Figure 6 of Bertschinger 1985). Note however that at late times, these streams, especially the outward moving ones, become rather chaotic. This is a result of an instability in the spherical infall model first described by Henriksen & Widrow (1997). In contrast, the gas particles are decelerated with $v_r \to 0$ for $r \to 0$. The presence of an outward moving shock is clearly seen in Figure 2 where we plot the temperature T as a function of r for frames (b) and (d) of Figure 1.

We next turn to vorticity. In SPH one determines the evolution of a fluid system by following the motion of fiducial particles which are labeled with local kinematic and thermodynamic quantities

(for a review, see Monaghan 1992 and references therein). Any function $f(\mathbf{r})$ of these quantities may be approximated by the following summation:

$$f(\mathbf{r}) = \sum_{b=1}^{N} \frac{m_b}{\rho_b} W(\mathbf{r} - \mathbf{r}_b; R) f_b \tag{19}$$

where f_b is the value of $f(\mathbf{r})$ for the b'th particle and

$$\rho_b = \sum_{b=1}^{N} m_b W(\mathbf{r} - \mathbf{r}_b; R) \tag{20}$$

In these expressions, W is a user-supplied window function with characteristic radius R. This measurement process introduces an error which can be minimized (but not eliminated) by an appropriate choice of R. Quantities that involve gradients require a bit more care and the measurement prescription is not always unique. Following Monaghan (1992) the vorticity is determined as follows:

$$\boldsymbol{\omega}_a = (\boldsymbol{\nabla} \times \mathbf{v})_a = \frac{1}{\rho_a} \sum_{b=1}^{N} m_b \mathbf{v}_{ba} \times \boldsymbol{\nabla}_a W_{ab} \tag{21}$$

where $\mathbf{v}_{ba} \equiv \mathbf{v}_b - \mathbf{v}_a$, $W_{ab} \equiv W(\mathbf{r}_a - \mathbf{r_b}; R)$ and $\boldsymbol{\nabla}_a W_{ab}$ denotes the gradient of W_{ab} with respect to $\mathbf{r}_a$. Following the usual practice, we choose the $\mathbf{r}_a$ to be the positions of the particles themselves though in principle $\mathbf{r}_a$ can be taken to be at any point in the simulation volume.

In addition to the measurement error discussed above, there is an error associated with the integration of particle orbits. Moreover, the "boxy" nature of the particle distribution, an artifact of the initial conditions, will lead to vorticity generation even with $q = 1$ since we do not have true spherical symmetry.

As a diagnostic test of these potential difficulties we determine the vorticity field in the spherical run discussed above. The result is shown in Figure 3 where we plot the (r, θ, ϕ) components of the measured $\boldsymbol{\omega}$ as a function of r for frame (b) of Figure 1. The large θ and ϕ components imply that there are angular gradients in v_r and/or radial gradients in v_θ and v_ϕ. For exact spherical symmetry and properly treated gasdynamics, the velocity fields should be purely radial and the only gradients in the r direction. ω_θ and ω_ϕ represent the first terms that arise when spherical symmetry is broken. In contrast, a nonzero ω_r requires angular gradients in the tangential velocity field and is therefore second order in small quantities and so it is not surprising that the measured ω_r is the smallest of the three components. As expected, the amplitudes of ω_θ and ω_ϕ decrease with increasing particle number, roughly as $N^{-1/3}$.

As mentioned above, errors are introduced into the vorticity calculation simply because we are attempting to determine a continuous field from information at discrete and irregularly spaced points. In order to quantify this aspect of the problem, we calculate the vorticity for a distribution of particles with the same positions as those used to generate Figure 3 but with velocities chosen by hand to reproduce a prescribed velocity field. Equation 21 is then used to determine the

"measured" vorticity field. For this experiment, we assume a prescribed velocity field of the form $v_z = \left(x^2 + y^2\right)^{1/2}$ which implies a constant vorticity field, $\boldsymbol{\omega} = \hat{\boldsymbol{\phi}}$. The measured field, shown in Figure 4, indicates that for most particles, the SPH prescription does a good job of calculating the vorticity. However, for a subset of particles, errors of order unity are introduced.

The difficulties inherent in following the generation and evolution of vorticity in hydrodynamic simulations is apparent in the simulations of Kulsrud et al. (1997). They determine the magnetic field by solving eq. 3 with the additional term eq. 5 included on the right hand side. As a check, they compare the result with the vorticity (scaled by the appropriate constant) and find discrepancies of order unity (cf. their Figure 4).

We next calculated the vorticity for the prolate protogalaxy simulation (Figure 5). As expected, there is now significant vorticity generated at the shock, primarily in the azimuthal direction. The vorticity in the r and θ directions is again an artifact of the simulation. The rms of ω_ϕ is a factor of 5 greater than that of ω_θ and ω_r. This can be viewed, in some sense, as a measure of the signal-to-noise of the simulation.

In Figure 6, ω_ϕ is plotted as a function of θ. The expected antisymmetry about the equatorial plane ($\theta = \pi/2$) is readily apparent. In particular, the vorticity near the poles ($\theta = 0$ and π) vanishes. However, we also find that there is vorticity generated with the "wrong sign", i.e., $\omega_\phi < 0$ for $0 < \theta < \pi/2$ and $\omega_\phi > 0$ for $\pi/2 < \theta < \pi$. This can be understood as follows: When the gas flows through the shock, it is refracted away from the symmetry axis and toward the equatorial plane. This leads to a region of high pressure and density in the equatorial plane forcing the gas to move out along the symmetry axis and creating a region of vorticity with the opposite sign. This is illustrated in Figures 7a and 7b where we show the velocity field of the particles in the simulation.

For a system mass of $7 \times 10^{11} M_\odot$, corresponding to a spiral galaxy roughly the size of the Milky Way. The magnitude of the vorticity is $\simeq 10^{-15}\,\mathrm{s}^{-1}$ in good agreement with our earlier estimate. The magnitude of the corresponding magnetic field is $\simeq 10^{-19}\,\mathrm{G}$. The protogalaxy at these early stages is roughly 25 kpc in size whereas the actual disk will have a radius $\sim 10\,\mathrm{kpc}$ and a thickness $\sim 1\,\mathrm{kpc}$. Contraction of the protogalaxy in the plane of the disk will therefore amplify the seed field by a factor of $(25/10)^2 \simeq 6$ while collapse perpendicular to this plane will amplify the field by a factor ~ 25 (Lesch & Chiba 1995). We therefore expect a field strength in the fully assembled disk galaxy of $1.5 \times 10^{-17}\,\mathrm{Gauss}$. This is approximately what is required to seed the galactic dynamo.

An alternative scenario is to generate the first magnetic fields in $10^6\,M_\odot$ objects. The seed fields are approximately two orders of magnitude larger (see Table 1). More importantly, the dynamical time for these systems is significantly shorter. It may therefore be possible for dynamo action to amplify fields on these scales before the disk is assembled.

4. Post-Shock Evolution

In the axisymmetric model described above, the vorticity and magnetic field generated at the shock are in the azimuthal direction and are antisymmetric about the equatorial plane. Mixing of gas from above and below this plane will lead to a rapid decrease in the vorticity, a reflection of the fact that angular momentum has not been included. The evolution of the magnetic field involves recombination and is therefore more complicated. It is however clear that no large-scale coherent field will survive without the addition of angular momentum. As discussed above, shear angular momentum is generated by tidal interactions with neighboring protogalaxies and is typically oriented along one of the short axes of the protogalaxy. It is the action of the shear field on the vorticity and magnetic fields that leads ultimately to a dipole configuration for these fields. This process can be illustrated by the following simple calculation. A set of particles are used to represent fluid elements labeled by their position, velocity, velocity gradient, and magnetic field. We assume force-free evolution so that each particle evolves independently according to the following (Cartesian coordinate) equations:

$$\frac{dx_i}{dt} = v_i \qquad \frac{dv_i}{dt} = 0 \tag{22}$$

$$\frac{d\partial_i v_j}{dt} = (\partial_i v_k)(\partial_k v_j) \qquad \frac{dB_i}{dt} = B_j \partial_j v_i - B_i \partial_j v_j \tag{23}$$

Initially, the magnetic field is in the azimuthal direction and is antisymmetric about the equatorial (xz) plane (Figure 8a). The prescribed velocity field includes shear angular momentum about the z-axis and an inward radial flow. The latter is meant to model the continual contraction of the fluid under the influence of gravity. After a short period of time, these field lines are sheared into a dipole configuration (Figure 8b).

5. Conclusions

In summary, we have presented a detailed investigation of magnetic field generation during the collapse of a protogalactic density perturbation. The first fields appear, via the Biermann battery effect, in the region of the outward moving shock that develops in the collapsing protogalaxy. Shear angular momentum is then able to reconfigure the field into a dipole pattern oriented along the spin axis of the protogalaxy. The predicted field strength, once the disk has formed, is estimated to be 10^{-17} Gauss. With a seed field of this magnitude, dynamo action can create microgauss fields by the current epoch. The magnitude of the associated vorticity at the time of disk formation is roughly equal to its present day value.

Virtually all galactic dynamo models assume azimuthal symmetry with respect to the spin axis of the disk. The dynamo equations in these models possess an invariance with respect to reflections about the equatorial plane and therefore the solutions can be divided into two groups: odd modes which consist of a dipole-like poloidal field together with an antisymmetric toroidal field and even modes which consist of quadrupole-like poloidal fields together with symmetric toroidal fields. In

general, even modes are favored (faster growing) when the fields are confined to a disk, while odd modes are favored in more spherical configurations (e.g., Ruzmaikin, Shukurov, & Sokoloff 1988). Observations would seem to indicate that both types of configurations are present in nature: The fields in the inner regions of the Milky Way, for example, appear to be predominantly antisymmetric with respect to the disk plane (Han et al. 1997) while those in M31 are evidently symmetric (Han, Beck, & Berkhuijsen 1998).

Our analysis suggests that dipole-like seed fields are favored (see, also Krause & Beck 1998). However, in a more realistic model, based on hierarchical clustering, we expect both dipolar and quadupolar fields to be produced.

If galactic magnetic fields have their origin in the Biermann battery effect operating in protogalactic shocks, it should be possible to follow the formation of a disk galaxy from primordial density perturbation, with $\mathbf{B} = 0$, to mature galaxy with a microgauss field. Our analysis and simulations have taken the first step in this ambitious program. Future work will include cosmological tidal fields as well as small scale perturbations. In addition, the magnetic field will have to be treated explicitly since the correspondence with vorticity is ultimately lost.

We wish to thank R. Henriksen, H. Couchman, and, L. Chamandy for useful discussions. LMW acknowledges the hospitality of The University of Chicago during a sabbatical stay and GD acknowledges the hospitality of the Canadian Institute for Theoretical Astrophysics. This work was supported in part by a grant from the Natural Sciences and Engineering Research Council of Canada.

REFERENCES

Bertschinger, E. 1985, ApJS, 58, 39

Biermann, L. 1950, *Zs. Naturforsch.*, 5a, 65

Binney, J. J. and Merrifield, M. 1998 *Galactic Astronomy* (Princeton, NJ: Princeton University Press)

Bisnovatyi-Kogan, G. S., Ruzmaikin, A. A., and Syunyaev, R. A. 1973, Sov. Ast. 17, 137

Carlberg, R. G. and Dubinski, J. 1991, ApJ, 369, 13

Couchman, H. M. P., Thomas, P. A. , Pearce, F. R. 1995, ApJ, 452, 797

Dalcanton, J. Spergel, D., and Summers, F. 1997, ApJ, 482, 659

Eisenstein, D. J. and Hu, W. 1999, ApJ, 511, 5

Fall, S. M. and Efstathiou, G. 1980, MNRAS, 193, 189

Field, G. B. and Carroll, S. M., 1998, astro-ph/9811206

Fillmore, J. A. and Goldreich, P. 1984, ApJ, 281, 1

Gott, J. R. 1975, ApJ, 201, 296

Gunn, J. E. 1977, ApJ, 218, 592

Han, J. L., Manchester, R. N., Berkhuijsen, E. M., and Beck, R. 1997, A&A, 322, 98

Han, J. L., Beck, R., and Berkhuijsen, E. M., 1998, A&A, 335, 1117

Harrison, E. R. 1970, MNRAS, 147, 279

Harrison, E. R. 1973, Phys. Rev. Lett., 30, 18

Henriksen, R. N. and Widrow, L. M. 1997, Phys. Rev. Lett., 78, 3426

Hoyle, F. 1949, in *Proc. Symposium on Motion of Gaseous Masses of Cosmical Dimensions, Problems of Cosmical Aerodynamics*, ed. J. M. Burgers and H. C. van de Hulst (Dayton: Central Air Documents Office), p. 195

Katz, N. and Gunn, J. E. 1991, ApJ, 377, 365

Kim, E.-J., Olinto, A. V., and Rosner, R. 1996, ApJ, 468, 28

Krause, F. and Beck, R. 1998, A&A, 335, 789

Kronberg, P. P. 1994, Rep. Prog. Phys. 325

Kulsrud, R. M., Cen, R., Ostriker, J. P. and Ryu, D. 1997, 480, 481

Landau, L. D. and Lifshitz, E. M. 1959, *Fluid Mechanics* (London: Pergamon Press)

Lesch, H. and Chiba, M. 1995, A&A , 297, 305

Mestel, L. 1963, MNRAS, 126, 553

Monaghan, J. J. 1992, ARA&A, 30, 543

Peebles, P. J. E. 1969, ApJ, 155, 393

Pudritz, R. E. and Silk, J. 1989, ApJ, 342, 650

Quashnock, J., Loeb, A. and Spergel, D. 1989, ApJ, 344, L49

Ratra, B. 1992, ApJ, 391, L1

Rees, M. J. QJRAS, 1987, 28, 197

Ryden, B. S. 1988, ApJ, 329, 589

Ryden, B. S. and Gunn, J. E. 1987, ApJ, 318, 15

Ruzmaiken, A. A., Shukurov, A. M., and Sokoloff, D. D. 1988, in Astrophysics and Space Science Library, Magnetic Fields in Galaxies (Dordrecht: Kluwer)

Sicotte, H. 1997, MNRAS, 287, 1

Turner, M. S. and Widrow, L. M. 1988, Phys. Rev. D37, 2743

Warren, M. S., Zurek, W. H., Quinn, P. J., and Salmon, J. K. 1992, ApJ, 399, 405

Wasserman, I. 1978, ApJ, 224, 337

White, S. D. M. 1984, ApJ, 286, 38

Vachaspati, T. 1991, Phys. Lett. B, 265, 258

Zel'dovich, Ya. B., Ruzmaikin, A. A., and Sokoloff, D. D. 1983, Magnetic Fields in Astrophysics, Gordon and Breach, New York

Table 1. Physical units for numerical simulations

$[M]$ $M_\odot$	10^6	10^9	7×10^{11}
z_i [a]	120	63	25
z_f [b]	43	22	8.4
$[L]$ (kpc)	5.9	11	24
$[V]$ ($\mathrm{km\,s^{-1}}$)	14	100	560
$[\omega]$ ($10^{-16}\mathrm{s^{-1}}$)	75	29	7.5
$[B]$ (10^{-20} G)	79	31	7.9

[a]Redshift at the start of the simulation

[a]Redshift corresponding to panel (d) of Figure 1

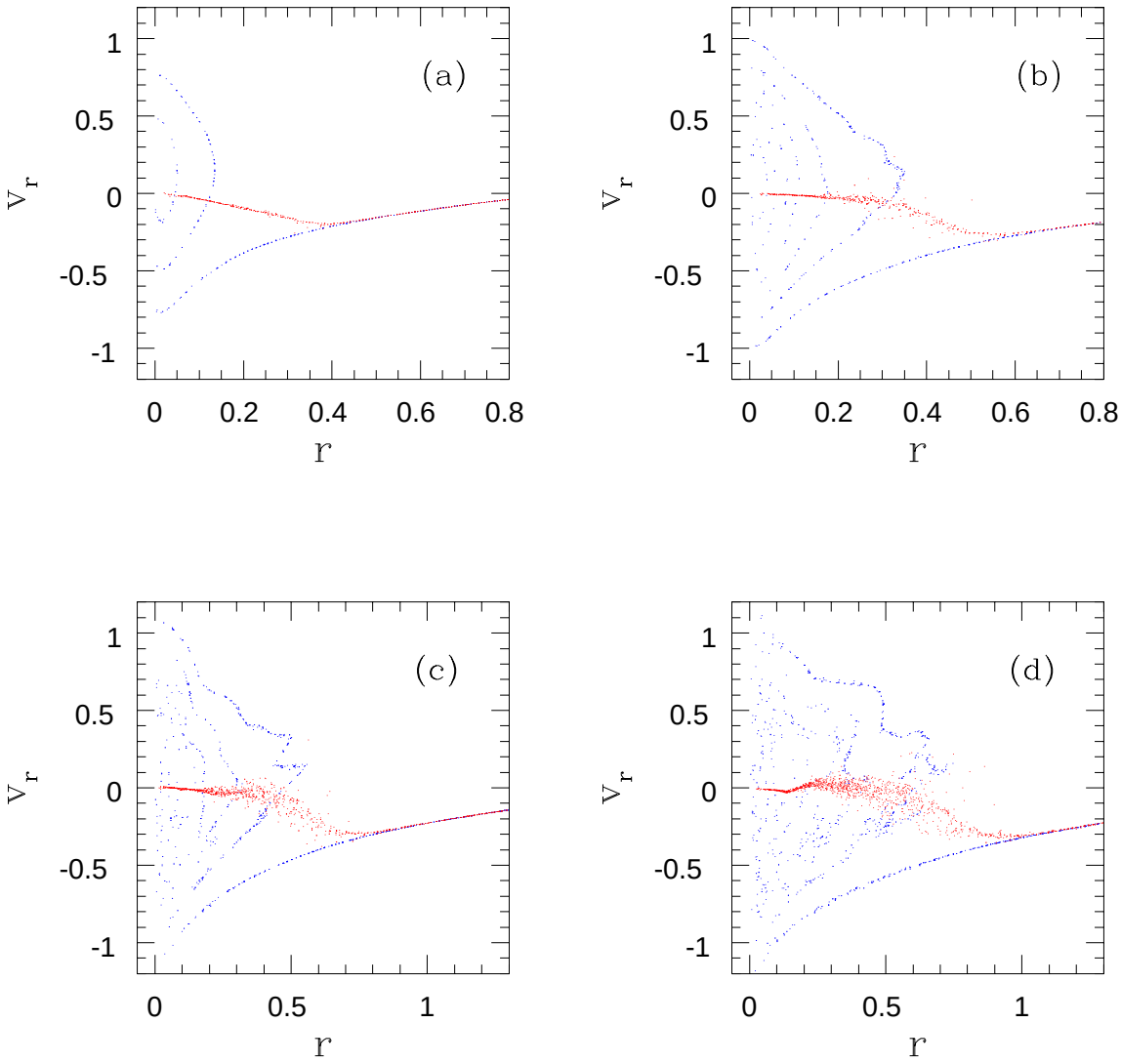

Fig. 1.— Phase space (radius r vs. radial velocity v_r) distribution of particles in the spherical run. The blue points represent dark matter particles while the red points represent gas particles.

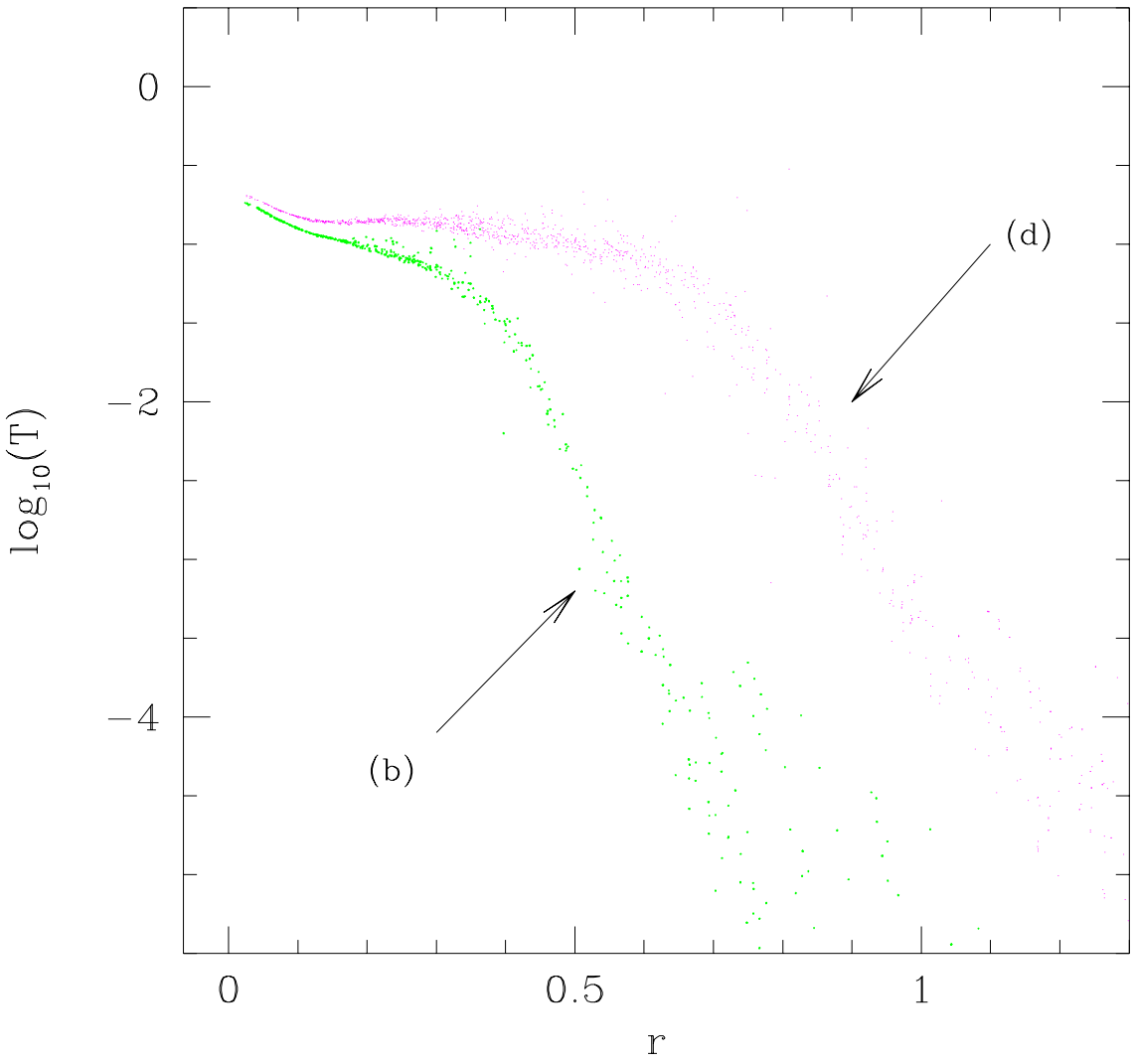

Fig. 2.— Temperature as a function of radius corresponding to frames (b) and (d) of figure 1

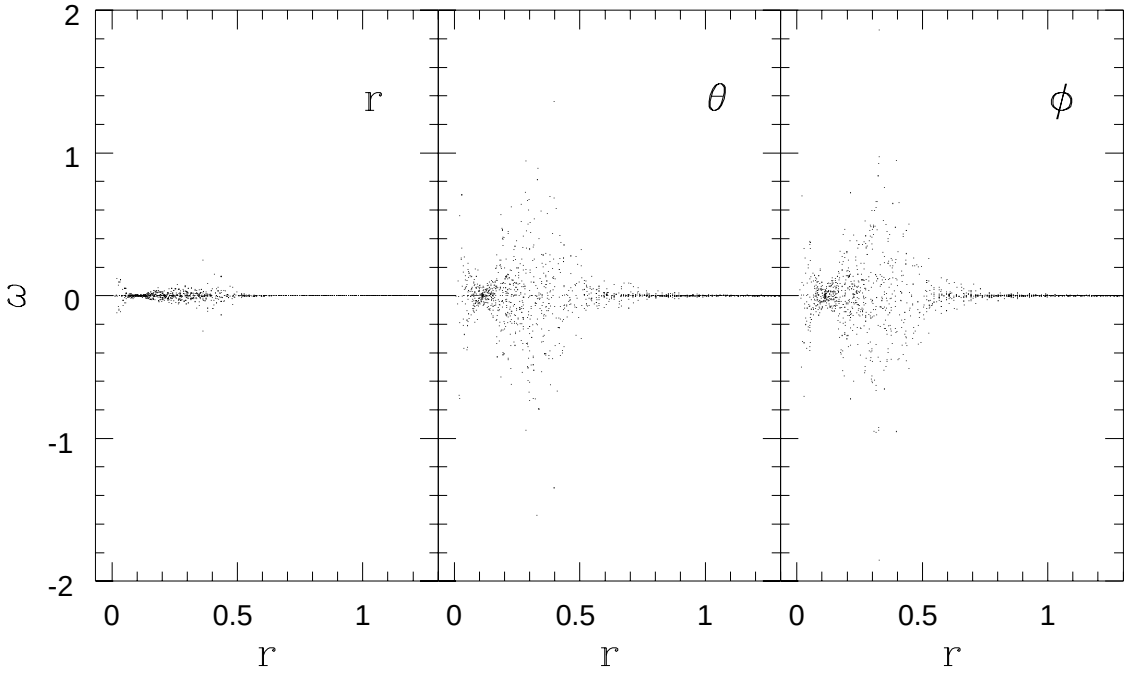

Fig. 3.— (r, θ, ϕ) components of $\boldsymbol{\omega}$ for frame (b) of Figure 1.

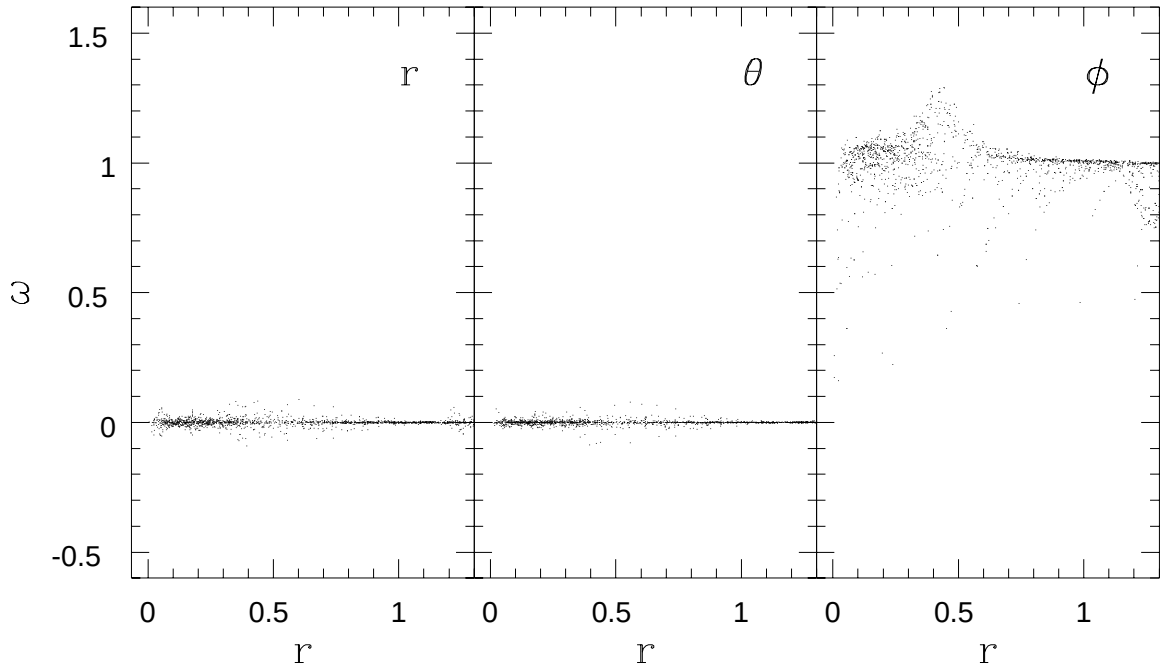

Fig. 4.— Same as Figure 3 with a prescribed velocity field corresponding to $\boldsymbol{\omega} = \hat{\boldsymbol{\phi}}$.

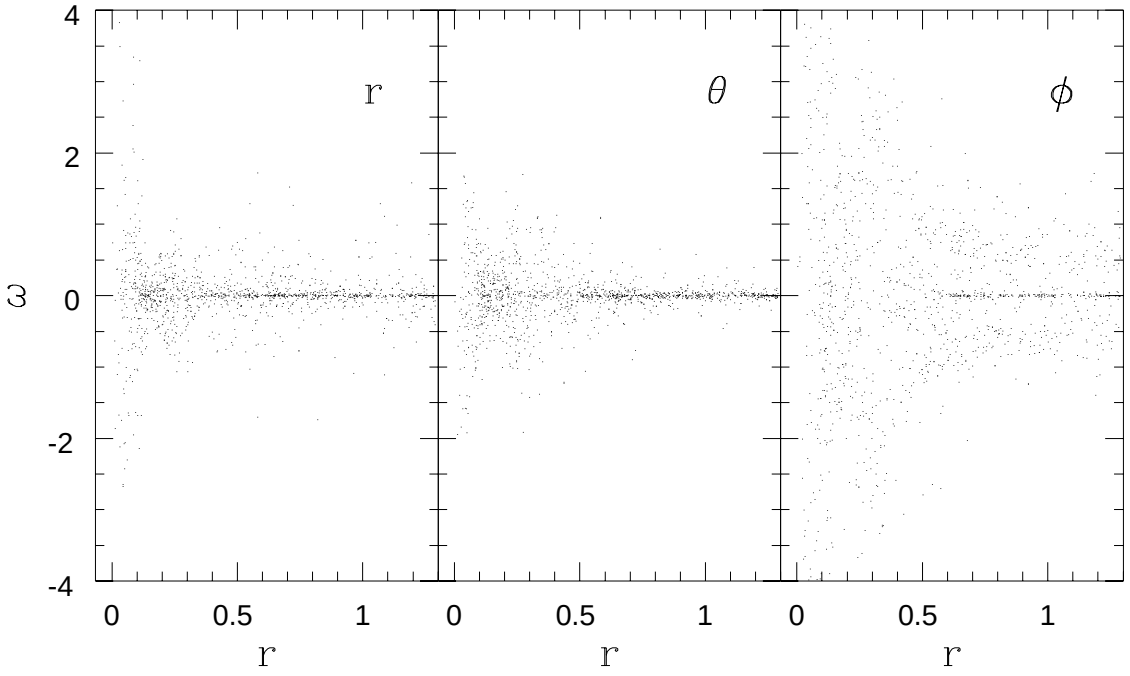

Fig. 5.— Same as Figure 3 but for the prolate protogalaxy ($q = 1.5$).

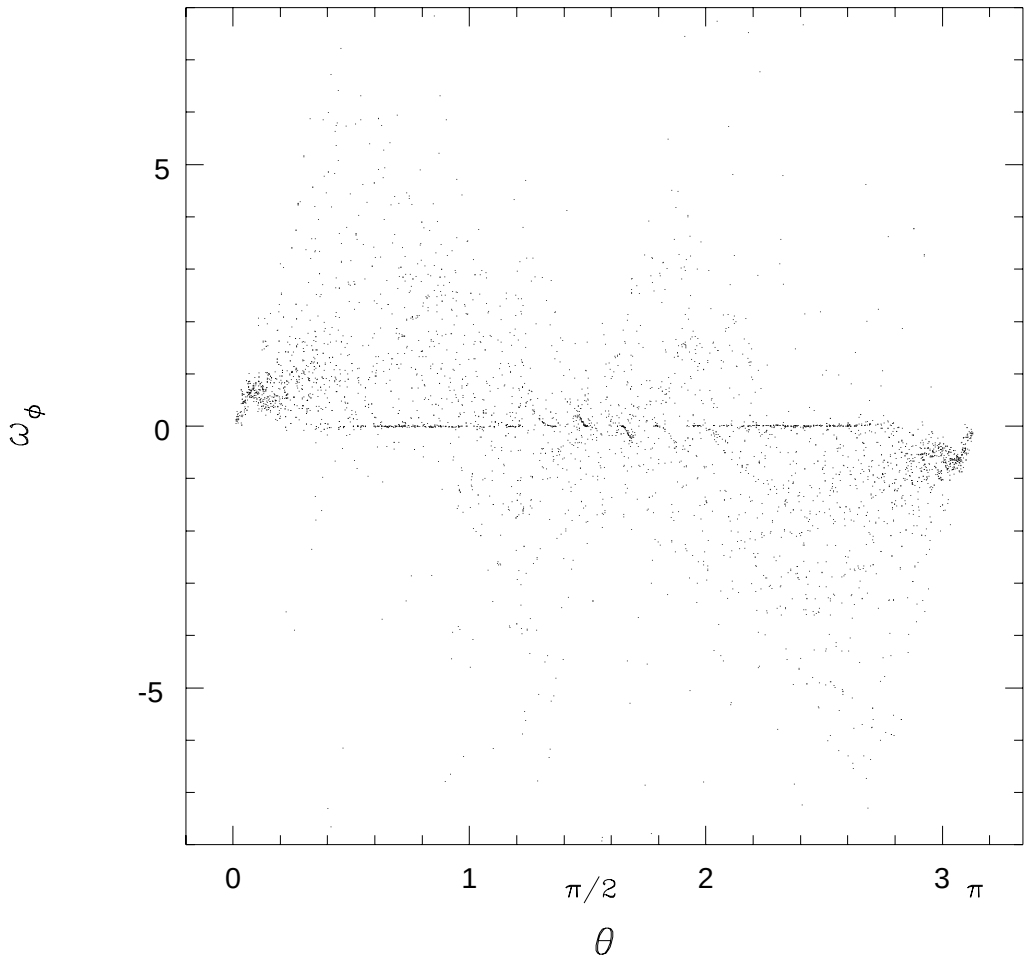

Fig. 6.— ω_ϕ as a function of θ.

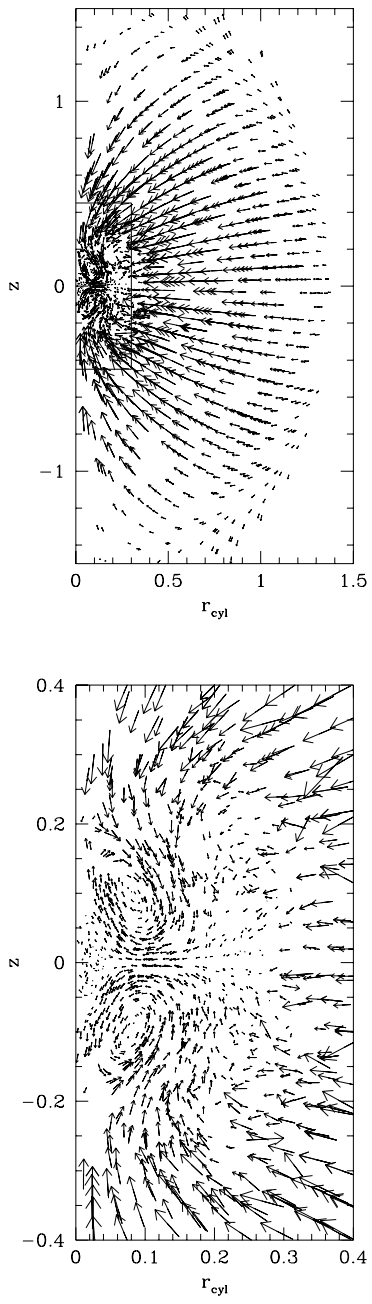

Fig. 7.— Velocity field for a prolate protogalaxy ($q = 1.25$) as a function of cylindrical radius r and position along the symmetry axis z. (a) The entire protogalaxy. (b) Inner region of the protogalaxy corresponding to the rectangular box in (a).

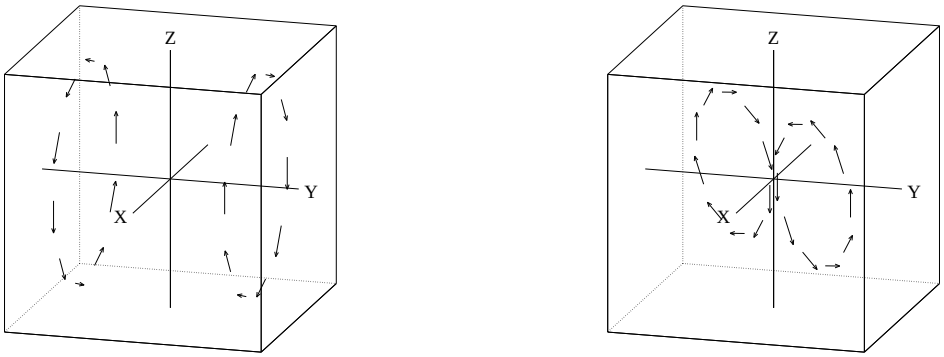

Fig. 8.— Magnetic field in the Lagrangian calculation described in Section 4. (a) The initial field configuration. The symmetry axis of the protogalaxy coincides with the y-axis. (b) Final configuration. Particles have evolved under the influence of a shear field that has net angular momentum in the z direction.